Models of stochastic biperiodic oscillations and extended serial correlations in electroreceptors of paddlefish

Alexander B. Neiman*
Department of Physics and Astronomy, Ohio University, Ohio 45701, USA

David F. Russell†
Center for Neurodynamics, University of Missouri at St. Louis, St. Louis, Missouri 63121, USA
(Received 3 February 2005; published 23 June 2005)

Two types of minimal models were used to study stochastic oscillations in sensory receptors composed of two coupled oscillators, as in the electroreceptors of paddlefish. They have populations of cells in sensory epithelia undergoing ≈26 Hz oscillations. These are coupled unidirectionally via synaptic excitation to a few afferent neurons, each of whose terminal contains a 30–70 Hz oscillator, expressed as a dominant peak in the power spectra of spontaneous afferent firing, corresponding to the mean firing rate. The two distinct types of internal noisy oscillators result in stochastic biperiodic firing patterns of the primary afferent sensory neurons. However, the functions of the oscillations have remained elusive, motivating this study. The models we used here are based on the circle map, or on the Ermentraut-Koppell canonical phase (theta neuron) model. Parameters were chosen according to experimental data. We used the models to demonstrate that the presence of epithelial oscillations leads to extended negative correlations of afferent interspike intervals, and to show that the correlation structure depends crucially on the ratio of the afferent to epithelial oscillation frequencies, being most pronounced when this ratio is close to 2, as observed in experiments. Our studies of stochastic versions of these models are of general interest for a wide range of coupled excitable systems, especially for understanding the functional roles of noisy oscillations in auditory and other types of "hair cell–primary afferent" sensory receptors.

DOI: 10.1103/PhysRevE.71.061915 PACS number(s): 87.19.La, 05.45.Xt, 87.17.Nn, 87.19.Nn

I. INTRODUCTION

Many sensory receptors possess a structure whereby detector cells in a sensory epithelium are synaptically coupled to one or more excitable primary afferent neurons. The sensory epithelia are composed of stimulus-sensitive hair cells separated by support cells. The afferent axon conducts action potentials, a receptor's output, to the brain. Examples of such "hair cell–primary afferent" receptors include the auditory and vestibular sensory receptors of vertebrates, and also the electroreceptors of certain aquatic animals.

Prominent examples of spontaneous oscillations in hair cells have been characterized, occurring without any stimulus being applied [1–4]. The oscillations are expressed as periodic shifts of the membrane potential of a hair cell, or as periodic motions of a hair cell's mechanosensitive cilia. The natural frequency of oscillations correlates with the stimulus frequency that a given hair cell is most sensitive to, thus contributing to frequency selectivity [1,3]. It was proposed recently that spontaneous oscillations in certain auditory hair cells are "active," in other words, are not simply driven by thermal noise [4,5].

On the other hand, spontaneous oscillatory firing patterns of afferent neurons have been observed in several sensory receptors. For example, mammalian cold receptor afferents produce repetitive bursts of spikes when chilled [6]; the oscillations have been modeled as arising from slow ion channels in the afferent terminals [7,8].

In this paper, we use minimal models to characterize and explore the possible function of two distinct types of oscillators embedded into the novel "biperiodic" organization of electroreceptors (ERs) of paddlefish (*Polyodon spathula*) [9,10]. An ER of this freshwater fish offers an accessible and experimentally advantageous biological model for studying nonlinear phenomena such as self-sustained oscillations [9], synchronization [11], bursting, and noise-induced phenomena [12,13]. Thousands of electrosensitive organs are located on an elongated appendage called the rostrum, located in front of the head. The rostrum acts as an antenna for detecting weak electrical signals emitted by planktonic prey [12,14]. A single ER is a system consisting of a cluster of 3–35 skin pores (Fig. 1), each leading into a short canal [15], which ends in a sensory epithelium containing ≈400 hair cells. The hair cells of a cluster synaptically excite the terminals of a few (2–4) primary afferent sensory neurons, whose axons project to the brain. The population of epithelial cells generates stochastic oscillations at approximately 26 Hz, expressed as a noisy oscillatory field voltage that can be recorded from ER canals. Collectively we term this the "epithelial oscillator" (EO). The EO is coupled unidirectionally via synaptic excitation to another oscillator, residing in each afferent's terminal, and driving spikes. The latter "afferent oscillator" (AO) has a natural frequency in the 30–70 Hz band, depending on the particular ER, and is expressed as a dominant peak in power spectra of spontaneous afferent firing. Afferent spectra also show a noisy peak at the

*Electronic address: neiman@helios.phy.ohiou.edu
†Electronic address: drussell@admiral.umsl.edu

 ©2005 The American Physical Society

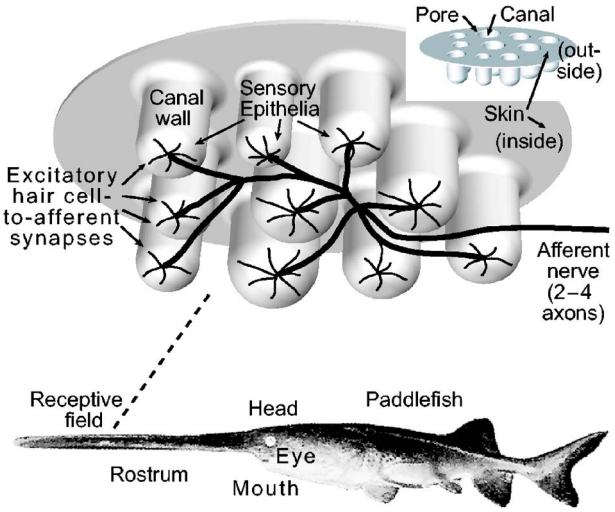

FIG. 1. Organization of electroreceptors (ERs) on the rostrum of paddlefish. They are of the ampullary cathodally excited type, like ERs in sharks and rays. Each short (0.2 mm) canal leads from a 0.1 mm diameter pore on the skin to a sensory epithelium, containing voltage-sensitive hair cells. The canals in a single receptive field form a cluster, approx. 2 mm in diameter. All of the epithelia in the cluster are innervated by 2–4 afferent sensory neurons, whose axons conduct action potentials to the brain.

EO frequency [9,10], due to the hair-cell–to–afferent synaptic input [15]. Both types of oscillators influence the pattern of afferent firing, which, as a result, is stochastically biperiodic or quasiperiodic.

A detailed study of cellular mechanisms of paddlefish ERs is not available yet, and thus a detailed ionic model of an ER system cannot be constructed at this time. Nevertheless, to investigate the functions of biperiodic organization, we propose minimal formal models for the spontaneous stochastic oscillations and biperiodicity observed in paddlefish ERs. The first and most general model is a circle map. This model has been widely studied in the mathematical literature, and is a generic model for a periodically driven self-sustained oscillator. The second model is based on the Ermentrout-Koppell canonical phase model, or so-called theta neuron model, which describes type-I spiking or excitability [16]. We include an additional noisy periodic modulation of a control parameter, to incorporate the EO.

Using these models, we studied the impact of epithelial oscillators on the statistical properties of afferent firing, seeking to delineate possible advantages of internal oscillators and biperiodic organization for the operation of hair cell–primary afferent sensory receptors in general, as well as paddlefish ERs. In particular, we explored possible origins of the extended negative correlations of afferent interspike intervals (ISIs) that have been observed in experimental data. Recently, in another type of ER found in weakly electric fish [17–19], it was shown that anticorrelations of ISIs, lasting for only a few ISIs, lead to regularity of P afferents on intermediate time scales ($\approx$200 msec) and give rise to increased ER sensitivity [17]. In general, ISI correlations have been attributed either to internal dynamics of a neuron, such as slow adaptation currents, or to external correlated input [20,21]. We observe ISI anticorrelations in the afferent firing of paddlefish ERs, but the anticorrelations are more extended, continuing for up to 50 ISIs [9,10]. We show here that the extended duration of ISI anticorrelations in a paddlefish ER is due to its biperiodic structure, based on our experimental evidence for the existence of epithelial and afferent oscillators [9,10], and the known hair-cell–to–afferent coupling [15]. Furthermore, we present experimental and modeling results showing that the structure of the ISI serial correlations is determined by the ratio of the frequencies of the EO and the AO.

The paper is organized as follows. In Sec. II we review experimental results on spontaneous activity of electroreceptors. Sections III and IV are devoted to the circle map and to the phase models, respectively.

II. STATISTICAL PROPERTIES OF OSCILLATIONS IN PADDLEFISH ELECTRORECEPTORS

Epithelial oscillations result from the collective activity of hundreds of cells in the epithelial layer at the bottom of a canal. Their summed voltage activity, as recorded using a single pipet electrode inserted into a canal's skin pore, we refer to as the EO. Remarkably, the fundamental frequency of the EO in different canals and in different fish is very similar (26 ± 1.6 Hz), at the regulated temperature of 22 °C [10]. We will employ this fact further on, using the period of the EO, $T_e=1/f_e=1/26$ sec, as a reference time scale for modeling of ERs. The EO processes in different canals of the same ER are uncorrelated [10]. The epithelial oscillations are closely akin to Gaussian narrowband or "harmonic" noise [22]. Since 3–35 epithelia converge synaptically onto a given afferent, then the EO input to an afferent is a sum of 3–35 uncorrelated stochastic oscillatory processes of similar frequency.

In contrast to the EO, the fundamental frequency of the afferent oscillator, estimated as the mean spontaneous firing rate or from the fundamental peak in power spectra of spontaneous firing, was distributed over a wide range of 30–70 Hz for different afferents in different fish [10], at 22 °C. For a given afferent, the smoothed firing rate was relatively fixed, and the probability density of interspike intervals had a γ-like shape with a well-expressed single peak. The coefficient of variation (CV), defined as the ratio of the standard deviation of the ISI to the mean ISI, $c_v=\sqrt{\langle\tau^2\rangle-\langle\tau\rangle^2}/\langle\tau\rangle$, was in the range of 0.1 to 0.38 [10]. However, since CVs and probability density distributions of ISIs are invariant for simple shuffling of interspike intervals, these commonly used neuroscience metrics do not provide information about the correlation structure of afferent spiking.

Stimulation with external electric fields revealed another striking feature of ERs. Only the AO frequency was affected by weak external electric stimuli, while the frequency of epithelial oscillations was almost invariant [10]. Inhibitory step stimuli of large enough amplitude can stop the afferent firing, which then returns (adapts) back to normal with a gradually increasing firing rate. During slow inhibitory linear ramp stimuli, the firing rate can be gradually decreased down to

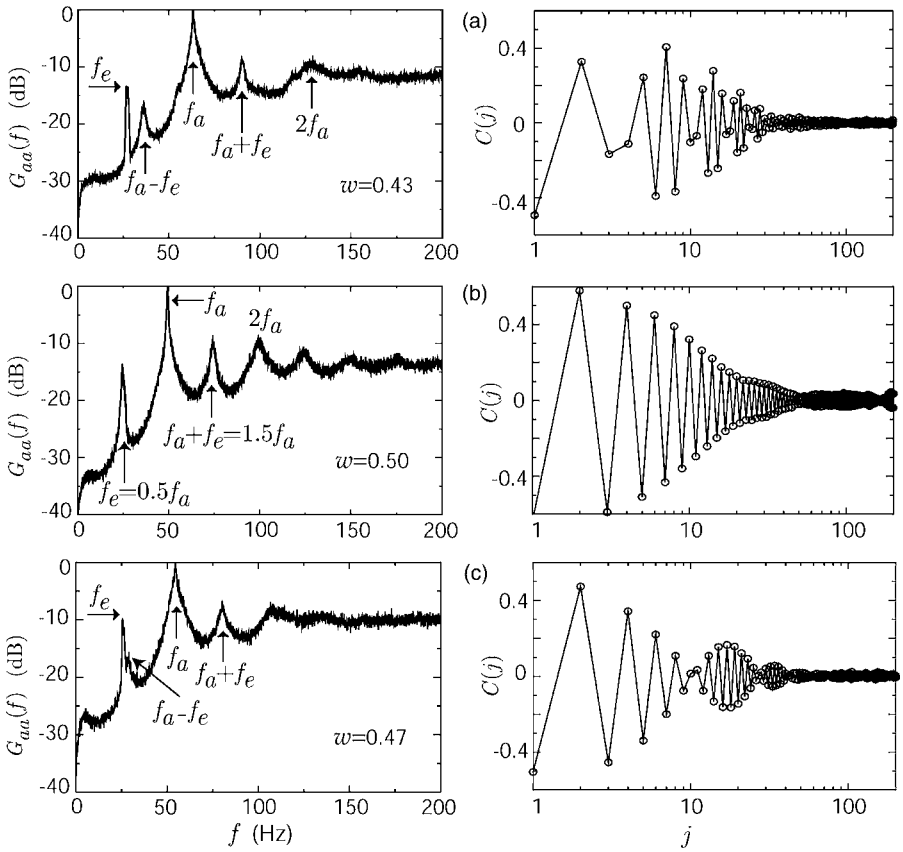

FIG. 2. Experimental data from paddlefish electroreceptor afferents. Left column: Power spectra calculated from spike trains recorded from three different primary afferents (a),(b),(c). Values of the epithelial-to-afferent frequency ratio w are listed. Right column: Serial correlation coefficients (SCCs) of the same spike trains.

zero. These experimental observations suggest that the afferents conform to the so-called type-I neuronal spiking [16,23].

Power spectra of spontaneous afferent firing showed a specific structure expected for a periodically driven nonlinear oscillator (see Fig. 2). The main peak at f_a corresponded to the mean firing rate of the afferent. An independent peak at f_e corresponded to the frequency of epithelial oscillations, since it matched the fundamental peak in the power spectrum of a canal signal from the afferent's receptive field. Sidebands at $f_a \pm f_e$ and higher harmonics of these peaks were always present. The mean EO:AO ratio of their fundamental frequencies during spontaneous activity, $w=f_e/f_a$, was 0.49 ± 0.08, estimated from power spectrum peaks of 67 afferents [10]. This ratio was relatively fixed in a given afferent. That is, the EO and the AO were often close to being in a 1:2 rational frequency ratio.

In the *absence of epithelial oscillations*, e.g., in aged preparations in which the EO amplitude had run down, afferent firing became nearly periodic [9]: its power spectrum showed only a narrow sharp peak at the mean firing rate (and its higher harmonics). Thus, epithelial oscillations can be considered as *internal noise* for the ER system. This noise, however, is narrowband, and leads to the existence of correlations between interspike intervals, as seen in the f_e peak and sideband peaks in afferent power spectra.

An effective metric of correlations between sequential ISIs, $\tau_n = t_n - t_{n-1}$, is the autocorrelation function of interspike intervals, also known as the serial correlation coefficient (SCC), defined as

$$C(j) = \frac{\langle \tau_k \tau_{k+j} \rangle - \langle \tau_k \rangle^2}{\langle \tau_k^2 \rangle - \langle \tau_k \rangle^2}, \tag{1}$$

where j is the lag after a given ISI in terms of the number of elapsed ISIs. The SCC (1) measures linear relations between sequential interspike intervals, and ranges from -1 (anticorrelation) to $+1$ (complete correlation). In the case of a renewal point process, $C(j)=\delta_{j,0}$, where $\delta_{j,0}$ is the Kronecker symbol. The SCC can be characterized by a single number, the correlation time (or correlation length) t_{cor} [24], which in our case can be calculated as

$$t_{cor} = \sum_{j=1}^{\infty} |C(j)|. \tag{2}$$

The SCCs in Fig. 2 (right column) clearly illustrate the nonrenewal character of the underlying stochastic point processes. The SCCs showed oscillatory character, since there was usually a negative correlation between the duration of sequential ISIs. That is, a long ISI tended to be followed by a short ISI, and vice versa [10,25,26], such that the ISI variability was reduced when considering pairs of spikes [17–19].

A new result is illustrated in Fig. 2: the structure of the SCC depends on the ratio w of the fundamental frequencies of the two oscillators. The longest correlations observed in Fig. 2(b) corresponded to the ratio $w \approx 0.5$ between the frequencies of the afferent and epithelial oscillators, that is, at the rational mode locking ratio 1:2. In other examples, the SCC showed beating as in Fig. 2(c) when the frequency ratio

was slightly farther away from 0.5. At larger departures from $w=0.5$ [Fig. 2(a)], the anticorrelations were briefer and also smaller in magnitude.

The anticorrelations of spontaneous afferent ISIs in paddlefish ERs continue for an $\approx$10-fold larger number of ISIs (significant up to 50, sometimes more [9,10]) than those observed in P receptors of weakly electric fish [17,18], in which the anticorrelations propagate for only a few ISIs. Thus, we refer to the normal ISI anticorrelations in paddlefish ERs as being "extended." If the epithelial oscillations of paddlefish ERs were absent, as in aged preparations, the SCC of afferent ISIs still exhibited anticorrelations, but they vanished for lags greater than 2–3 interspike intervals [9], which we refer to as "short-term anticorrelations." The latter are probably an inherent property of the afferent terminal, and appear due to slow ionic currents, as in a model for P receptors of weakly electric fish [18]. In P receptors, these short-term anticorrelations act to decrease the spectral power at low frequencies in afferent power spectra [21,27].

Our experimental data showing that the tenfold extension of ISI anticorrelations is due to interactions of the EO and AO include the following: (1) correlation between the presence or absence of the EO and the presence or absence (respectively) of extended ISI anticorrelations; (2) dependence of the structure and length of ISI anticorrelations on the EO:AO frequency ratio in different receptors; and (3) ability to evoke prompt increases in the ISI correlation length by experimentally increasing the EO amplitude [9], or vice versa, in a given receptor. Based on results from P receptors, we expect the extension of ISI anticorrelations to have several functional effects: reduce higher-order variability, increase sensitivity, decrease in spectral power at low frequencies in afferent power spectra, and increase in effective "memory" in the stochastic point processes of paddlefish ER afferents.

III. PHASE RELATIONS BETWEEN THE TWO OSCILLATORS: CIRCLE MAP MODEL

The circle map is the generic model to study quasiperiodicity and synchronization in periodically driven or coupled self-sustained oscillators [28–30]. The circle map establishes a correspondence between the phase of an oscillator at a moment of time $t=t_0$ and the phase at $t=t_0+T$, where T is the period of an external driving force [30]: $\psi_{n+1}=\psi_n+2\pi f_0 T+KF(\psi_n)$, where f_0 is the unperturbed frequency of the oscillator, $F(\psi)$ is a 2π-periodic function, and the parameter K refers to the coupling (driving) strength. A generalization of the circle map model leads to the concept of the annulus map [30], which was recently derived and studied in Ref. [31] for a periodically driven leaky integrate-and-fire model with a threshold fatigue.

Simultaneous recording from a paddlefish ER afferent and a canal in the afferent's corresponding receptive field allowed the phase relations between them to be characterized [10,32]. The phase $\psi(t)$ of a canal signal $s(t)$ was estimated using the concept of an analytic signal [33]. The instantaneous phase of canal oscillations can then be calculated at the spike times t_n of the afferent, $\psi_n=\psi(t=t_n)$. The next step was to build a map $\psi_{n+1}=F(\psi_n)$ which served as an analog of the circle map [28,29]. As further simplification, we can consider the EO as a periodic signal driving the AO, such that ψ_n represents the phase of the EO at the moment of nth firing of the afferent neuron: $\psi_n=2\pi f_e t_n$, where f_e is the fundamental frequency of the epithelial oscillator and t_n is the firing time of the nth afferent spike. The corresponding circle map reads

$$\psi_{n+1}=2\pi\rho+\psi_n+KF(\psi_n). \tag{3}$$

The parameter K corresponds to the amplitude of the epithelial oscillations. The parameter ρ determines the ratio of frequency of the unperturbed AO (e.g., when $K=0$) to the frequency of the EO: $\rho=f_e/f_a^0$, where f_a^0 is the frequency of AO in the absence of driving from the EO. The resulting frequency ratio f_e/f_a is given by the winding number [30]:

$$w=\frac{f_e}{f_a}=\lim_{n\to\infty}\frac{\psi_n-\psi_0}{2\pi n}. \tag{4}$$

We can rewrite the circle map Eq. (3) explicitly for the afferent spike times t_n:

$$f_e t_{n+1}=\rho+f_e t_n+\frac{K}{2\pi}F(2\pi f_e t), \tag{5}$$

where t_n are spike times in seconds. In terms of the dimensionless variable $\tilde{t}_n=f_e t_n$, we obtain

$$\tilde{t}_{n+1}=\rho+\tilde{t}_n+\frac{K}{2\pi}F(2\pi\tilde{t}_n), \tag{6}$$

where spike times are now measured in units of the period of the EO, $T_e=1/f_e$. With the first two harmonics taken into account, $F(\psi)=\sin(\psi)+\alpha\sin(2\psi)$, the circle map has the form

$$\tilde{t}_{n+1}=\rho+\tilde{t}_n+\frac{K}{2\pi}[\sin(2\pi\tilde{t}_n)+\alpha\sin(4\pi\tilde{t}_n)]+D\xi_n. \tag{7}$$

In Eq. (7), we introduced Gaussian white noise ξ_n with intensity D to account for stochastic variability in the AO [34]. The second harmonic was introduced to avoid a degeneracy of the period-2 cycle of the ISI $\tau_n=t_n-t_{n-1}$ when $\rho=0.5$. In the following we will use $\alpha=-0.15$ for all calculations.

A continuous-time afferent spike train can be constructed from a sequence t_n generated by Eq. (7) as $a(t)=\Sigma_n\delta(t-t_n)$, where the spike times were renormalized back to dimension units $t_n=T_e\tilde{t}_n$ with $T_e=1/26$ sec for comparison with experimental results. The power spectrum can be calculated in the same way as for experimental data [10]: δ functions were approximated by a rectangular pulse centered at t_n, and with a width $\Delta t=5\times10^{-5}$ sec, corresponding to a sampling rate of 20 kHz. Power spectra were then estimated using the fast Fourier transform, with averaging over overlapping windows of length $\Delta t\times 2^{18}=13.1$ sec.

Figure 3 shows three examples of power spectra and the SCCs calculated from the circle map (7). The structure of the model's power spectrum closely resembles spectra from experimental spike trains (see Fig. 2): there are two fundamental peaks at f_e and f_a, and sidebands. However, power spectra from the circle map always display δ peaks at the EO fun-

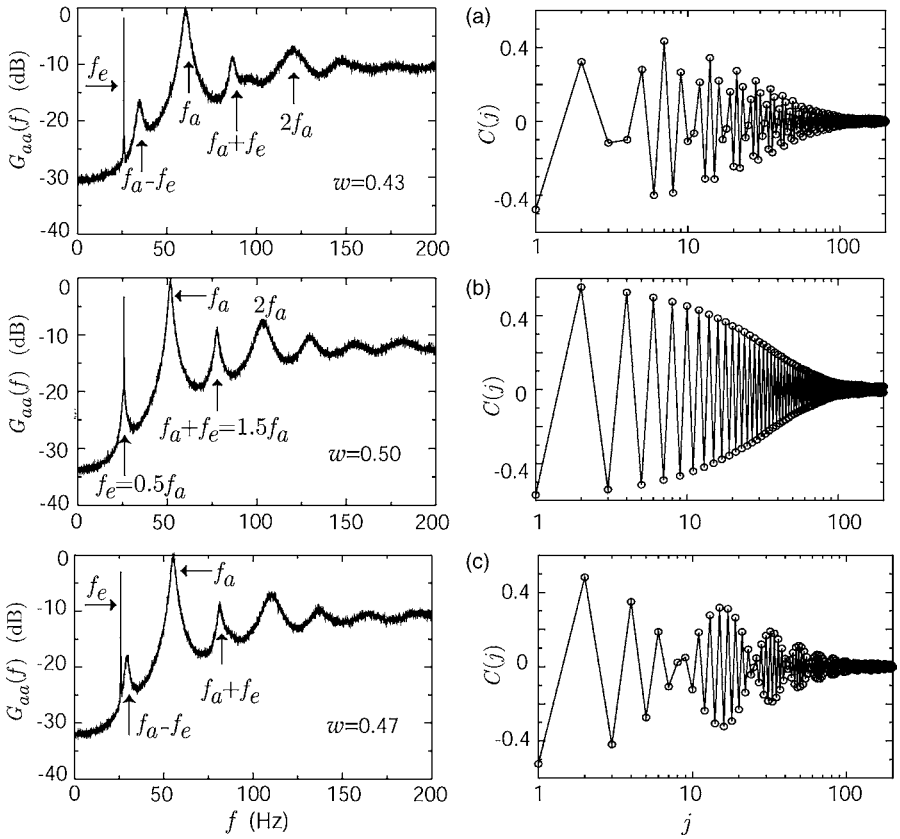

FIG. 3. Power spectra (left column) and corresponding SCCs (right column) for spike trains generated by the circle map model (7) with parameters chosen to mimic experimental results as in Fig. 2. Values of the epithelial-to-afferent frequency ratio w are listed. The parameters were (a) $\rho=0.429$, $K=0.4$, $D=0.04$; (b) $\rho=0.5$, $K=0.4$, $D=0.04$; (c) $\rho=0.471$, $K=0.4$, $D=0.04$. The spike times were renormalized back to the dimension units $t_n=T_e\tilde{t}_n$.

damental frequency (f_e) and its higher harmonics, instead of finite-width peaks as in experimental power spectra. This is because the circle map implies a pure periodic driving, and thus does not take into account fluctuations in the EO. It is important to note that the structure of the SCC is determined by the frequency ratio w: the serial correlations are most pronounced when w is equal to 0.5, the case of 1:2 phase locking. For w close to 0.5, the SCC shows a beating structure, just as in experimental data [Fig. 2(c)].

As mentioned, a corresponding renewal process could be constructed from an ER afferent spike train by shuffling the sequence of ISIs, which destroys all correlations between intervals, while preserving the ISI distribution. Thus, this renewal process possesses the same mean ISI and CV as the original process.

To characterize in the frequency domain the impact of ISI correlations, we introduced the spectral ratio $S(f)$, calculated by dividing the afferent power spectrum $G_{aa}(f)$ by the power spectrum of the corresponding renewal process $G_{aa}^{shuf}(f)$:

$$S(f)=G_{aa}(f)/G_{aa}^{shuf}(f). \tag{8}$$

The spectral ratio at any given frequency is equal to 1 for a renewal process. The power spectrum at zero frequency can be related to the long-term variability and the SCC as [21,35,36]

$$G_{aa}(f=0)=\frac{c_v^2}{\langle\tau\rangle}\left(1+2\sum_{j=1}^{\infty}C(j)\right). \tag{9}$$

From the last formula, it is easy to see that the negative ISI correlations $[C(j)<0]$ lead to a loss of power at low frequencies, and to a decrease of long-term variability, and thus improve the performance of a sensory neuron for low-frequency (slow) stimuli [27]. The loss of power at low frequencies, due to ISI correlations, can be quantified by the value of the spectral ratio at zero frequency:

$$S_0=S(f=0)=\left(1+2\sum_{j=1}^{\infty}C(j)\right). \tag{10}$$

Thus, the spectral ratio characterizes the long-term variability of afferent firing as compared to a renewal process having the same mean firing rate and CV as the original spike train.

In the absence of periodic forcing ($K=0$), the circle map reduces to a linear discrete system, $\tilde{t}_{n+1}=\rho+\tilde{t}_n+D\xi_n$. In the case of white noise, this model describes a renewal process with $c_v=D/\rho$. With $K\neq 0$, the measures of variability become functions of both K and ρ, as well as the noise intensity D. In the absence of noise, $D=0$, the circle map possesses various mode-locking or synchronization regions (Arnold tongues) on the parameter plane (ρ,K) where the mode-locking $m:n$ regimes are stable. The borders of the Arnold tongues correspond to the saddle-node bifurcation transitions from $m:n$ periodic mode-locking cycles to a quasiperiodic motion with irrational winding numbers [28,30]. The influence of noise results in a shrinking of Arnold tongues [34]. However, the diffusion of an oscillator's phase is minimized inside the synchronization regions [30], and thus should lead to extended correlations.

We concentrate on the parameter region corresponding to a frequency ratio w near 0.5, as observed for paddlefish ERs. First, in Fig. 4, we show the dependence of the CV, the

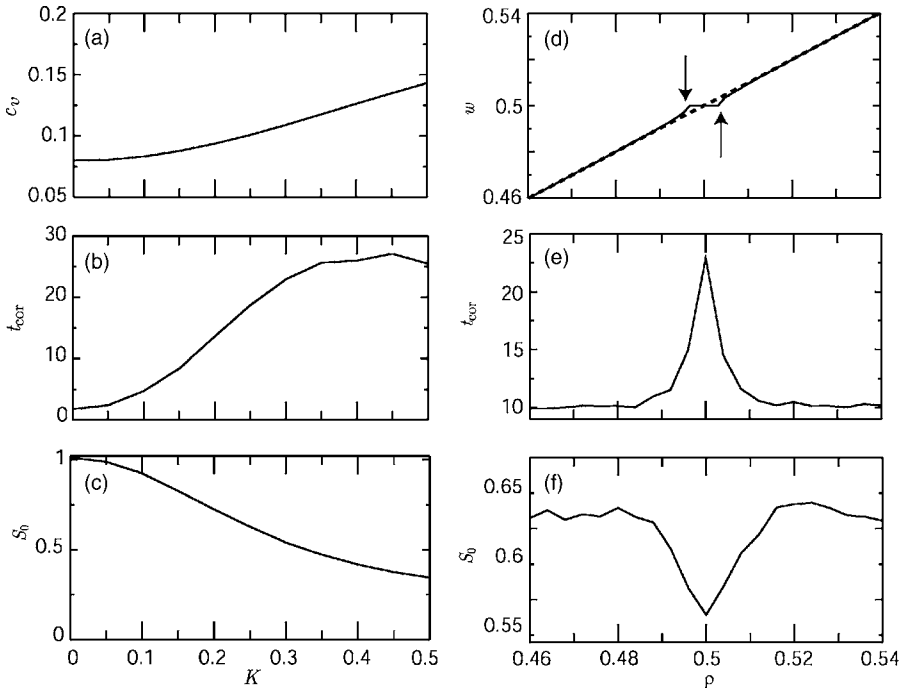

FIG. 4. Numerical simulations of the circle map (7). The dependence of CV (a), ISI correlation time (b), and the spectral ratio at zero frequency (c), versus the amplitude of the EO, K, at fixed $\rho=0.5$. (d)–(f) Dependence on the parameter ρ for the fixed values of $K=0.3$. (d) The frequency ratio w versus ρ. The solid line shows the deterministic case. Arrows point to the synchronization region, which is a flat segment when the frequency ratio equals 0.5. Dashed line corresponds to $D=0.04$. (e) ISI correlation time versus ρ. (f) Spectral ratio at zero frequency versus ρ. Noise intensity $D=0.04$.

correlation time, and the spectral ratio S_0 on the amplitude of the EO (parameter K) for various values of parameter $\rho=0.5$, and with fixed noise intensity. As in experimental data [9], the EO enhances variability of ISIs, expressed in terms of the CV: the CV increases with increasing K [Fig. 4(a)]. On the other hand, the EO reduces higher-order variability, since the ISI correlation time increases monotonically with K, and the spectral ratio S_0 decreases as the EO amplitude grows: both indicate that ISI correlations contribute to a loss of power at low frequencies.

Next, we vary the parameter ρ, keeping constant the EO and noise amplitudes. Both the correlation time [Fig. 4(e)] and the spectral ratio [Fig. 4(f)] undergo sharp extrema when ρ and the frequency ratio w pass through 0.5, which corresponds to the center of the 1:2 synchronization region (two afferent spikes per one cycle of epithelial oscillations).

These results from circle map models predict that correlation measures of ER afferent spike trains may undergo drastic changes when passing through synchronization regions, with extreme ISI correlation corresponding to a maximal loss of low-frequency power, occurring at $w=0.5$. Variation in w could be evoked by slow (in comparison with the periods of EO and AO) external stimuli, which could be introduced in the circle map model as variation of the parameter ρ.

IV. PHASE MODEL

A minimal model describing so-called type-I spiking and excitability is given by a canonical model (also known as the theta neuron model) [16,37,38], in which the neuron is described by a single phase variable θ:

$$\dot{\theta} = (1 - \cos\theta) + (1 + \cos\theta) r, \tag{11}$$

where r is the bifurcation parameter. For negative values of r, the model is excitable: it possesses two equilibria, $\theta^{\pm} = \pm\cos^{-1}[(1+r)/(1-r)]$, which are unstable and stable, respectively (see [39] for complete mathematical study). The equilibria $\theta^{\pm}$ merge at $r=0$, and for $r>0$ the model represents periodic spiking with the frequency $f_0=\sqrt{r}/\pi$. A spike is generated every time $\theta(t)$ crosses the value of π. The influence of white noise on the model was studied numerically in [40], and analytically in [41].

In our case of epithelia-afferent electroreceptors, the canonical model is used to mimic spontaneous firing of an afferent neuron, modulated by epithelial oscillations. To simplify consideration, we model the EO by a single stochastic self-sustained oscillator, and assume that it is described by only its phase $\psi(t)$:

$$\dot{\psi} = 2\pi\tilde{f}_e + \sqrt{2Q}\xi(t), \tag{12}$$

where $\tilde{f}_e$ is the (dimensionless) frequency of the EO, and $\xi(t)$ is zero-mean white Gaussian noise, with intensity Q, introduced to account for phase fluctuations. The EO signal is then described as $e(t)=\cos[\psi(t)]$, with the autocorrelation function $\langle e(t)e(t')\rangle = \exp(-|t-t'|Q)\cos[2\pi\tilde{f}_e(t-t')]$, and with a Lorentzian peak in its power spectrum, of width Q. Further on, we assume $\tilde{f}_e = 1/2\pi$. Indeed, alternate models for the EO are possible. For instance, a Gaussian narrowband noise (harmonic noise) [22] produces similar results. We introduce another Gaussian colored noise term $\eta(t)$ into Eq. (11) to account for the variability of the afferent firing in the absence of epithelial oscillations. Thus, our phase model is described by the following dimensionless equations:

$$\dot{\theta} = (1 - \cos\theta) + (1 + \cos\theta)[r + A\cos\psi + \sqrt{D}\eta(t)],$$

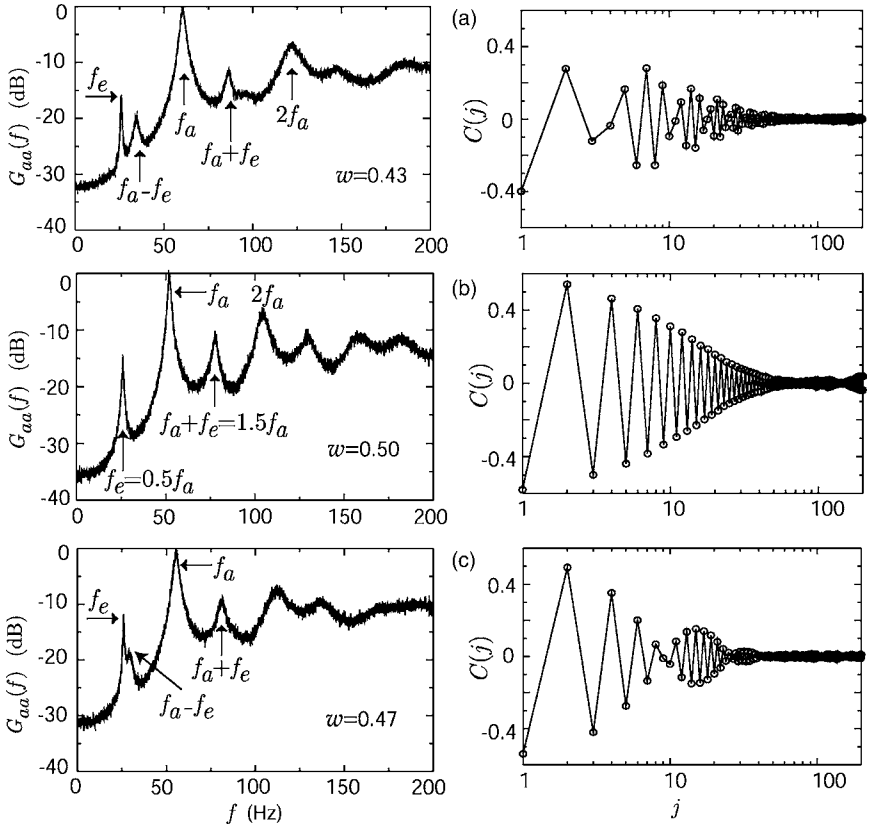

FIG. 5. Power spectra (left column) and corresponding SCCs (right column) for the numerically simulated phase model (13) with parameters chosen to produce the same frequency ratios w and the SCCs as in Figs. 2 and 3. Values of the epithelial-to-afferent frequency ratio w are listed. The parameters were (a) $r=1.365$, $A=0.35$, $D=0.05$, $Q=0.015$; (b) $r=1.015$, $A=0.3$, $D=0.02$, $Q=0.015$; (c) $r=1.155$, $A=0.4$, $D=0.04$, $Q=0.015$. The interspike intervals were renormalized to the period of the epithelial oscillator (see text) to obtain similar time scales as in experimental recordings.

$$\dot{\psi} = 1 + \sqrt{2Q}\xi(t). \tag{13}$$

In the model Eq. (13), the parameter A is the amplitude of the EO, and D is the intensity of Ornstein-Uhlenbeck Gaussian noise $\eta(t)$ with autocorrelation function $\langle \eta(t)\eta(t+t')\rangle = \gamma \exp(-\gamma|t-t'|)$ where $1/\gamma \ll 1$ is the noise correlation time. The noise sources $\eta(t)$ and $\xi(t)$ are statistically independent: $\langle \xi(t)\eta(t')\rangle = 0$. We set $\gamma = 100$ for all further numerical simulations. Since Eqs. (13) are dimensionless, in order to compare simulations with experimental results we renormalized the numerically obtained dimensionless spike time sequences $\tilde{t}_k, k=1,\ldots,N$, to spike times in seconds as $\tilde{t}_k/2\pi f_e$, with $f_e=26$ Hz. Numerical simulations of Eqs. (13) were conducted using the Euler scheme with the time step $\Delta t = 10^{-3}$, and the duration of simulation for each parameter value was equivalent to 10 min of experimental recording.

Numerical calculations of the power spectra, the SCCs, and the spectral ratios are shown in Fig. 5. In contrast to the circle map, the phase model Eqs. (13) takes into account fluctuations in the EO, which are reflected in a finite width of the EO power spectral line. The power spectrum had the same characteristic peaks as observed in experiments, and the SCCs showed experimentlike extended correlations.

The impact of serial correlations can be seen in Figs. 6(a)–6(c), where the spectral ratio was always less than 1 in the low-frequency domain. The SCC correlation time and the spectral ratio showed qualitatively the same behavior as for the circle map: at 1:2 mode locking, serial correlations showed maximal correlation time, while the spectral ratio attained its minimal value, indicating subtraction of power at low frequencies.

A closer look at the experimental power spectra (Fig. 2) and the spectral ratio [Fig. 6(d)] revealed differences from numerical simulations in the low-frequency domain: the experimental power decreased toward zero frequency, whereas in numerical simulation (Fig. 5) the power spectrum saturated in the low-frequency domain.

As discussed above, the experimental data still showed short-term negative serial correlations and corresponding low-frequency shaping of the power spectra [21] when the EO was absent (or of low amplitude). Such short-term negative correlations can be introduced into the canonical model by the addition of a slow adaptation variable $u(t)$:

$$\dot{\theta} = (1-\cos\theta) + (1+\cos\theta)[r + A\cos\psi + \sqrt{D}\eta(t) - u],$$

$$\dot{\psi} = 1 + \sqrt{2Q}\xi(t),$$

$$\dot{u} = -\lambda u + s\delta(\theta - \pi), \tag{14}$$

where $\lambda \ll 1$ and $s > 0$. Whenever a spike occurs, i.e., θ crosses π, the slow variable u undergoes a steplike increase, and then relaxes back to $u=0$. The negative character of the feedback delays the next firing, and thus results in adaptation to external stimuli [16,42]. For the leaky integrate-and-fire model, it was shown recently that such adaptation results in anticorrelations of ISIs [21]. The influence of short-term ISI anticorrelations on the power spectrum of a spike train is twofold [27]. First, anticorrelations lead to loss of low-frequency power, as was mentioned before. Second, anticor-

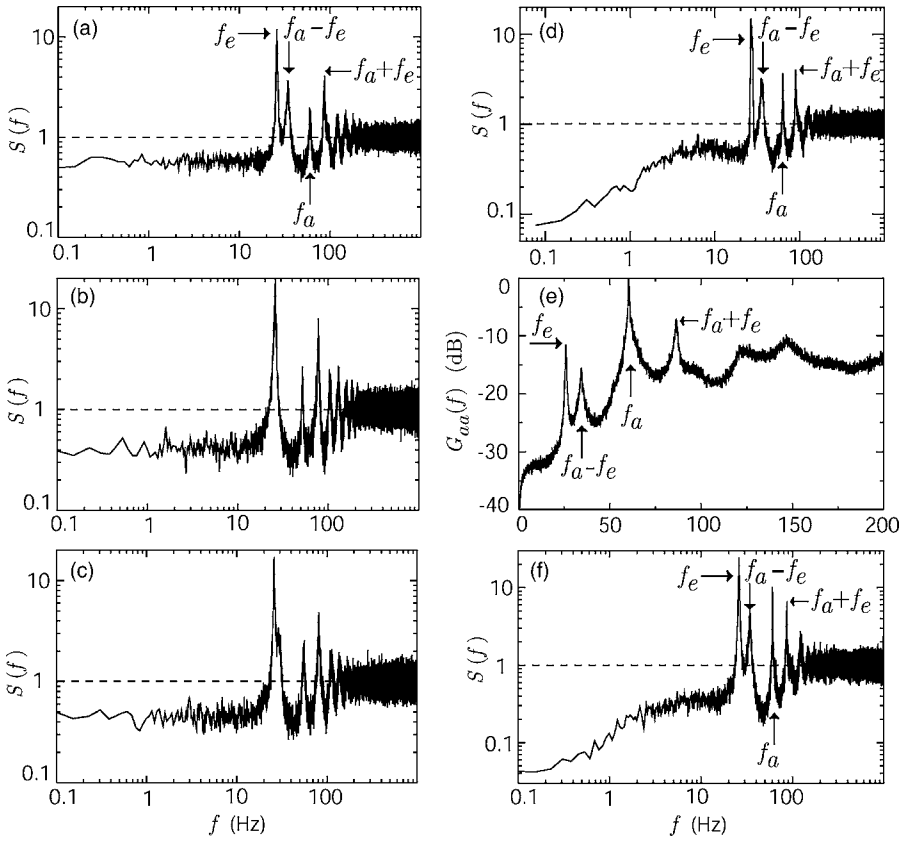

FIG. 6. (a)–(c) Spectral ratios $S(f)$ for the numerically simulated phase model (13) using the same parameters values as in panels (a)–(c) of Fig. 5. (d) Spectral ratio calculated from *experimentally* recorded spike train of the same ER afferent as in Fig. 2(a). (e),(f) Power spectrum and spectral ratio from numerical simulation of the phase model, with additional slow adaptation Eqs. (14). The parameters were $r=6.95$, $A=0.7$, $\lambda=0.02$, $s=0.3$, $D=0.06$, $Q=0.015$.

relations result in more coherent oscillations, expressed as a narrower spectral line at the fundamental frequency of the neuron [21]. Figures 6(e) and 6(f) illustrates this for numerical simulations of Eqs. (14). The power spectrum [Fig. 6(e)] possesses a narrower peak at the fundamental frequency of the AO, and there is less power at low frequencies, as compared to a renewal spike train. This shaping of the power spectrum is more apparent for the spectral ratio $S(f)$, plotted on a double logarithmic scale [Fig. 6(f)]: the spectral ratio is significantly less than 1 and declines toward 0 [note a very good agreement with experimental result for the spectral ratio shown in Fig. 6(d)].

V. CONCLUSION

We have used two generic models, the circle map and the phase canonical model, to study stochastic biperiodic oscillations in a sensory receptor system, paddlefish ERs, composed of two unidirectionally coupled oscillators. An oscillator residing in the primary afferent terminals (afferent oscillator) is influenced (synaptically excited) by another oscillator residing in the population of epithelial cells (epithelial oscillator). Experimental data from paddlefish electroreceptors were used to choose particular regimes and parameter values of the models.

The models used in this study generate nonrenewal spike trains with statistical properties, such as the power spectrum, and negative serial correlations, that reproduce well the experimental data from paddlefish ERs. The models show that the epithelial oscillator is responsible for the *extended* negative correlations of interspike intervals, as we also demonstrated experimentally [9,10]. Thus the mechanism of extended negative correlations is different from the mechanism of *short-term* negative correlations, like those observed in other sensory receptors [17–19,26], which can be introduced in the phase model via slow adaptation currents [20], acting like negative feedback [43]. Thus one prominent consequence of the biperiodic organization of paddlefish ERs is the generation of very long-lasting oscillatorylike ISI correlations.

In P receptors of weakly electric fish, *short* negative correlations arise in part due to phase locking of afferent spikes with the electric organ discharge. This is reflected in the negative slopes of clusters in ISI return maps [44]. Even so, the dominant effect of negative correlations was attributed to slow adaptation currents. Three different scales of correlations between interspike intervals of paddlefish ER afferents have been reported. First, the short-term anticorrelations observed even in the absence of epithelial oscillations [9] propagate for only a few spikes, lasting 50–100 msec, depending on the firing rate. They may be due to adaptation currents in afferent terminals, and resemble the anticorrelations in P receptors of weakly electric fish. Second, the extended anticorrelations studied here continue for 10–50 ISIs, lasting 200–1000 msec [9,10]. Third, long-range anticorrelations lasting 10–200 sec have been reported [45]. Our focus is the second of these, the extended anticorrelations, which we think are the most likely to be functionally significant.

The experimentally measured ratio of the fundamental frequencies of the epithelial and afferent oscillators was

0.49 ± 0.08 for 67 different paddlefish ERs [10]. Therefore the two oscillators embedded into an ER system operate near the strong 1:2 mode-locking regime. Our models predict that the statistical properties of the spike trains depend crucially on the frequency ratio of the two oscillators: the correlation time of the SCC is maximal when the ratio of the fundamental frequencies of two oscillators attains the rational number of 0.5. The increase of the correlation time corresponds to a decrease of ISI variability at low frequencies, seen as reduced spectral power in the low-frequency domain. We note that the frequency response of paddlefish ERs is maximal in the low-frequency range of 1 to 10 Hz [10], and thus a suppression of variability at low frequencies may enhance sensitivity of these ERs in an appropriate frequency range.

We can assume that spontaneous background activity of electroreceptors is used by the animal, in some unknown manner, as a reference to compare with a stimulus-altered spike train. While the frequency of the epithelial oscillator is invariant to weak external stimulation, the frequency of the afferent oscillator is easily changed by weak stimuli. For example, recalling that paddlefish use electrosense to locate zooplankton prey such as *Daphnia*, an approaching *Daphnia* passing along the rostrum with a constant speed generates a time-varying voltage gradient near an individual ER that generally has a bipolar wave form [46] and thus results in slow biphasic changes of firing rate of the ER afferent. This slow variation of afferent firing rate can be expected to lead to time-varying changes in the frequency ratio w, resulting in significant time-varying changes in the correlation statistics of the afferent spike train during the stimulus. After the stimulus has ceased (e.g., the *Daphnia* has passed out of range), the frequency ratio and ISI statistics return to the prestimulus state. We hypothesize that such prominent stimulus-induced changes in ISI statistics, resulting from the biperiodic organization of paddlefish ERs, convey information about a stimulus to the animal's brain for further processing.

ACKNOWLEDGEMENTS

We thank M. Chacron and B. Lindner for comments and valuable discussions. This work was supported by National Institutes of Health Grant No. DC04922.

[1] A. C. Crawford and R. Fettiplace, J. Physiol. (London) **364**, 359 (1985).
[2] A. Rüsch and U. Thurm, Hear. Res. **48**, 247 (1990).
[3] P. Martin, A. J. Hudspeth, and F. Jülicher, Proc. Natl. Acad. Sci. U.S.A. **98**, 14380 (2001).
[4] M. Ospeck, V. M. Eguiluz, and M. O. Magnasco, Biophys. J. **80**, 2597 (2001).
[5] S. Camelet, T. Duke, F. Jülicher, and J. Prost, Proc. Natl. Acad. Sci. U.S.A. **97**, 3183 (2000).
[6] H. Bade, H. A. Braun, and H. Hensel, Pfluegers Arch. **382**, 1 (1979).
[7] H. A. Braun, H. Wissing, K. Schäfer, and M. C. Hirsch, Nature (London) **367**, 270 (1979).
[8] H. A. Braun, M. T. Huber, M. Dewald, K. Schäfer, and K. Voigt, Int. J. Bifurcation Chaos Appl. Sci. Eng. **8**, 881 (1998).
[9] A. B. Neiman and D. F. Russell, Phys. Rev. Lett. **86**, 3443 (2001).
[10] A. B. Neiman and D. F. Russell, J. Neurophysiol. **92**, 492 (2004).
[11] A. Neiman, X. Pei, D. Russell, W. Wojtenek, L. Wilkens, F. Moss, H. Braun, M. Huber, and K. Voigt, Phys. Rev. Lett. **82**, 660 (1999).
[12] D. F. Russell, L. A. Wilkens, and F. Moss, Nature (London) **402**, 291 (1999).
[13] A. B. Neiman and D. F. Russell, Phys. Rev. Lett. **88**, 138103 (2002).
[14] L. A. Wilkens, D. F. Russell, X. Pei, and C. Gurgens, Proc. R. Soc. London, Ser. B **264**, 1723 (1997).
[15] J. M. Jørgensen, A. Flock, and J. Wersäll, Z. Zellforsch Mikrosk Anat. **130**, 362 (1972).
[16] E. M. Izhikevich, Int. J. Bifurcation Chaos Appl. Sci. Eng. **6**, 1171 (2000).
[17] R. Ratnam and M. Nelson, J. Neurosci. **20**, 6672 (2000).
[18] M. J. Chacron, A. Longtin, and L. Maler, J. Neurosci. **21**, 5328 (2001).
[19] J. B. M. Goense and R. Ratnam, J. Comp. Physiol., A **189**, 741 (2003).
[20] X.-J. Wang, J. Neurophysiol. **79**, 1549 (1998).
[21] B. Lindner and A. Longtin, Proc. SPIE **5114**, 209 (2003).
[22] L. Schimansky-Geier and C. Zülicke, Z. Phys. B: Condens. Matter **79**, 451 (1990).
[23] J. Rinzel and G. B. Ermentrout, *Analysis of Neural Excitability and Oscillations* (MIT Press, Cambridge, MA, 1998), pp. 313–360.
[24] R. L. Stratonovich, *Topics in the Theory of Random Noise* (Gordon and Breach, 1981).
[25] K. Schäfer, H. A. Braun, R. C. Peters, and F. Bretschnider, Pfluegers Arch. **429**, 378 (1995).
[26] M. C. Teich and S. B. Lowen, IEEE Eng. Med. Biol. Mag. **13**, 197 (1994).
[27] M. J. Chacron, B. Lindner, and A. Longtin, Phys. Rev. Lett. **92**, 080601 (2004).
[28] S. H. Strogatz, *Nonlinear Dynamics and Chaos* (Addison-Wesley, Reading, MA, 1995).
[29] L. Glass and M. C. Mackey, *From Clocks to Chaos: The Rythms of Life* (Princeton University Press, Princeton, NJ, 1988).
[30] A. S. Pikovsky, M. G. Rosenblum, and J. Kurths, *Synchronization: A Universal Concept in Nonlinear Sciences* (Cambridge University Press, Cambridge, U.K., 2001).
[31] M. J. Chacron, K. Pakdaman, and A. Longtin, Neural Comput. **15**, 253 (2003).
[32] M. Zeller, M. Bauer, and W. Martienssen, Chaos, Solitons Fractals **5**, 885 (1995).
[33] J. S. Bendat and A. G. Piersol, *Random Data: Analysis and Measurement Procedures* (J. Wiley and Sons, New York,

2000).
[34] A. B. Neiman, U. Feudel, and J. Kurths, J. Phys. A **28**, 2471 (1995).
[35] D. R. Cox and P. A. Lewis, *The Statistical Analysis of Series of Events* (Methuren, London, 1966).
[36] J. W. Middleton, M. J. Chacron, B. Lindner, and A. Longtin, Phys. Rev. E **68**, 021920 (2003).
[37] G. B. Ermentrout and N. Kopell, SIAM J. Appl. Math. **46**, 233 (1986).
[38] G. B. Ermentrout, Neural Comput. **8**, 979 (1996).
[39] F. C. Hoppensteadt and E. M. Izhikevich, *Weakly Connected Neural Networks* (Springer, Berlin, 1997).
[40] B. S. Gutkin and G. B. Ermentrout, Neural Comput. **10**, 1047 (1998).
[41] B. Lindner, A. Longtin, and A. Bulsara, Neural Comput. **15**, 1761 (2003).
[42] G. B. Ermentrout, Neural Comput. **10**, 1721 (1998).
[43] J. H. Shin, Neurocomputing **44**, 167 (2002).
[44] M. J. Chacron, A. Longtin, M. St-Hilaire, and L. Maler, Phys. Rev. Lett. **85**, 1576 (2000).
[45] S. Bahar, J. W. Kantelhardt, A. B. Neiman, H. Rego, D. F. Russell, L. A. Wilkens, A. Bunde, and F. Moss, Europhys. Lett. **56**, 454 (2001).
[46] W. Wojtenek, M. H. Hofmann, and L. A. Wilkens, Neurocomputing **38–40**, 451 (2001).